HHS Public Access

Author manuscript

Nat Cell Biol. Author manuscript; available in PMC 2014 November 01.

Published in final edited form as:

Nat Cell Biol. 2014 May ; 16(5): 401–414. doi:10.1038/ncb2934.

Connexins modulate autophagosome biogenesis

Eloy Bejarano[1], **Andrea Yuste**[1], **Bindi Patel**[1], **Randy F. Stout Jr**[2], **David C. Spray**[2], and **Ana Maria Cuervo**[1,*]

[1]Department of Developmental and Molecular Biology and Institute for Aging Studies, Albert Einstein College of Medicine, Bronx, NY 10461, USA

[2]Dominick P. Purpura Department of Neuroscience, Albert Einstein College of Medicine, Bronx, NY 10461, USA

Abstract

The plasma membrane contributes to formation of autophagosomes, the double-membrane vesicles that sequester cytosolic cargo and deliver it to lysosomes for degradation during autophagy. In this study, we have identified a regulatory role for connexins (Cx), main components of plasma membrane gap junctions, in autophagosome formation. We have found that plasma membrane-localised Cx proteins constitutively downregulate autophagy via a direct interaction with several autophagy-related proteins involved in the initial steps of autophagosome formation such as Atg16 and components of the PI3K autophagy initiation complex (Vps34, Beclin-1 and Vps15). On nutrient starvation, this inhibitory effect is released by the arrival of Atg14 to the Cx-Atg complex. This promotes the internalization of Cx-Atg along with Atg9, which is also recruited to the plasma membrane in response to starvation. Maturation of the Cx-containing pre-autophagosomes into autophagosomes leads to degradation of these endogenous inhibitors, allowing for sustained activation of autophagy.

Keywords

Autophagy; Connexins; Gap junctions; Lysosomes; Plasma membrane

*Corresponding author: Ana Maria Cuervo MD PhD, Department of Developmental and Molecular Biology, Albert Einstein College of Medicine, Bronx, NY, 10461, USA, ana-maria.cuervo@einstein.yu.edu.

Supplementary Information is linked to the online version of the paper

Author Contributions

EB designed and performed most of the experiments, analyzed the data and contributed to writing the paper; AY provided technical assistance with immunoblot and immunofluorescence and revised the written manuscript; BP performed the electron microscopy studies and morphometric analysis; RS performed live confocal imaging; DS provided feedback in experiment design, interpretation of the data and revised the written manuscript; AMC coordinated the study, designed experiments, analyzed data and contributed to the writing and revision of the paper.

Competing Financial Interest

The authors declare that they have no competing interests.

Introduction

Macroautophagy (hereafter referred to as autophagy) is responsible for the maintenance of cellular homeostasis through the continuous turnover of proteins and organelles in lysosomes[1] and participates in the cellular response to stress by eliminating damaged cellular structures and mobilizing intracellular energy stores. Alterations in this catabolic pathway have been linked to a growing number of human pathologies including cardiovascular diseases, neurodegeneration, microbial infection and cancer[2, 3].

The cytosolic material delivered to lysosomes for degradation by autophagy is first sequestered into double-membrane vesicles known as autophagosomes[4]. Organelles such as the endoplasmic reticulum, the mitochondria, the Golgi apparatus, the nuclear envelope and the plasma membrane (PM) and recycling endosomes have been shown to contribute to the formation of the autophagosome membrane[5–11]. In fact, autophagosome biogenesis requires the sequential assembly of autophagy-related proteins (Atg) that organize into functional complexes which come from different subcellular locations[4]. The earlier events involve the arrival of two different kinase protein complexes, the Beclin-1-Vps34-Vps15-Atg14 and the ULK1-Atg13-FIP200 complexes, and of the integral membrane protein Atg9[12–14]. Vps34-dependent phosphorylation of the lipids in specific intracellular membrane regions marks the site from where autophagosome membranes emerge and elongate through covalent conjugation of Atg5/Atg12/Atg16 and of LC3 with phosphatidylethanolamine (LC3-II)[15]. Although most of the proteins of the original donor membrane are excluded from the forming autophagosome, some of them may get incorporated into the limiting membrane of this organelle and undergo degradation through autophagy.

Autophagy contributes to the turnover of PM proteins[16–18] including surface receptors and structural components such as connexins (Cx), the multispan transmembrane proteins that assemble to form PM gap junctions[18–21]. The recent discovery that the PM is a site of autophagosome biogenesis motivated us to analyze whether Cx are incorporated in the forming autophagosome. In this work, we have found that Cx are present in autophagosome precursor structures that form prior to the formation of the autophagosome limiting membrane. In fact, Cx interact with a subset of Atgs at the PM and contribute to negatively modulate basal autophagy. Cx elimination or internalization from the PM is enough to upregulate autophagosome biogenesis and autophagy even in nutrient-rich conditions. Our study identifies Cx the regulated association of Atg14 and Atg9 to pre-existing Cx-Atg complexes at the PM as the trigger that neutralizes the Cx inhibitory effect through their internalization and degradation via autophagy.

Results

Connexin 43 associates to pre-autophagosomal structures

Cx can be detected in autophagosomes during nutrient starvation that induces their rapid internalization and autophagic degradation[18, 21] (Fig. 1a). We found an unusually high enrichment of Cx in autophagosomes that resembles the one of autophagosome structural proteins such as LC3-II (Fig. 1a and Supplementary Fig. 1a). In addition, more than 80% of isolated autophagosomes co-stained for Cx (Supplementary Fig. 1b).

Co-staining for Atg16 (a marker for pre-autophagosomal structures) and LC3 (a marker of the limiting membrane and autophagosomes) in cells expressing GFP-Cx43 (Fig. 1b and Supplementary Fig. 1c) or stained for endogenous Cx43 (Fig. 1c and Supplementary Fig. 1d, e) revealed the presence of this Cx in vesicles positive for both LC3 and Atg16, and also in Atg16-positive vesicles that did not stain for LC3. Cx43 did not colocalize under these conditions with Atg9 or Atg14, also involved in the early steps of autophagosome formation (Fig. 1c and Supplementary Fig. 1d). Activation of autophagy by serum removal (Fig. 1b) or blockage of autophagosome degradation with an inhibitor of lysosomal proteolysis (Fig. 1c and Supplementary Fig. 1d, e) both increased the amount of Cx43 in LC3 positive vesicles, but did not increase Cx43 colocalization with Atg16. Time-lapse microscopy and 3D reconstruction confirmed the presence of Atg16 at PM Cx-enriched gap junction (GJ) (Fig. 1d and Supplementary Fig. 1f) that markedly increased when Cx43 internalization was blocked (i.e. Eps15 knock-down[22] ; Fig 1e).

A pool of Atg16 co-immunoprecipitated with Cx43 and *vice versa* (Fig. 1f) even after activation of autophagy by serum removal (Fig. 1g). Clathrin, shown to bind Atg16 at the PM[8] could also be detected in the Cx43 pull-downs albeit at lower levels than Atg16 (Fig. 1g). In contrast, LC3 was not retrieved with Cx43 (Fig. 1g), suggesting that although both proteins localize in autophagosomes, they do not interact in theses compartments. Atg16 and Cx43 interaction was still observed upon pharmacological (3-methyladenine treatment) or genetic (Atg5−/− cells) inhibition of autophagy (Fig. 1h, Supplementary Fig. 1g; efficacy of treatments is shown in Supplementary Fig. 2a, b). Atg5 was not recovered as part of the Atg16-Cx43 complex (Supplementary Fig. 1h), suggesting that these two proteins interact before autophagy activation occurs. We found that Cx43 interacts at the Atg16 C-terminus (Fig. 1i) whereas Atg5 binds the Atg16 N-terminus (Supplementary Fig. 1i). Overall, we conclude that a fraction of Cx43 interacts with Atg16 before nucleation and limiting membrane elongation occurs.

Cx43 negatively modulates autophagy

To elucidate the functional relevance of the observed interaction of Cx43 with pre-autophagosome structures we used mouse osteoblasts (MOB) from wild type (Wt) and Cx43-null mice ($Cx43^{-/-}$)[23]. Cells lacking Cx43 had higher: 1) number of LC3-positive puncta in nutrient-rich media (Fig. 2a) that further increased upon serum removal (Supplementary Fig. 2c); 2) number of GABARAP positive vesicles (Fig. 2a)[24]; 3) number of electron microscopic profiles compatible with autophagic vacuoles[25] (Fig. 2b and Supplementary Fig. 2d); and 4) steady-state levels of LC3-II (Fig. 2c). Higher number of autophagic vesicles in $Cx43^{-/-}$ likely reflects increased biogenesis rather than reduced lysosomal clearance because the percentage of autophagosomes (pre-lysosomal fusion) and autophagolysosomes (post-lysosomal fusion) in these cells did not differ from Wt cells (Supplementary Fig. 2d). Furthermore, $Cx43^{-/-}$ cells displayed higher fluxes of LC3 (LC3-II accumulation upon lysosomal proteolysis inhibition) and higher increases in the levels of LC3-II at two different times upon proteolysis blockage (when any increase in LC3-II can only result from autophagosome synthesis) (Fig. 2c). Similar increases in autophagosome formation and autophagic flux in $Cx43^{-/-}$ cells were observed using the mCherry-GFP-LC3 reporter that allows tracking autophagosome/lysosome fusion as an increase in red

fluorescence puncta (GFP fluorescence decreases at low pH)[26] (Fig. 2d). Electron microscopy of $Cx43^{+/-}$ mice livers revealed a significant increase in the number and size of autophagic vacuoles (mostly autophagolysosomes) (Fig. 2e and Supplementary Fig. 2e, f) confirming that Cx43 deficit leads to constitutive autophagy activation also *in vivo*. Expression of GFP-Cx43 in $Cx43^{-/-}$ cells was enough to partially suppress the induction of basal autophagy (Fig. 2f, g) whereas overexpression of Cx43 in control MEFs consistently reduced autophagic flux (Supplementary Fig. 2g).

Overall these results support a previously unknown role of Cx43 as an endogenous negative regulator of autophagosome formation.

Cx43-dependent inhibition of autophagy does not require functional GJ communication

Because one of the key functions of PM Cx is their role in intracellular communication, we tried to recapitulate the upregulation of autophagy observed in Cx-deficient cells with the potent GJ inhibitor 18α glycyrrhetinic acid (GA)[27] that disrupts Cx arrangement within GJ, without affecting PM localization[28] (Supplementary Fig. 3a). Chemical inhibition of GJ function led to a discrete increase in the steady-state levels of LC3-II and LC3-positive puncta, but contrary to Cx ablation, autophagic flux was reduced (Fig. 3a, b). A similar effect was noted in $Cx43^{-/-}$ cells (Fig. 3a) suggesting that these changes were independent of Cx. Inhibition of GJ function did not change levels of Atg16-positive vesicles (Supplementary Fig. 3b, c) or Cx association with these pre-autophagosome structures (Supplementary Fig. 3d). Therefore, the constitutive inhibitory effect of Cx over autophagy may not depend on their role in intercellular communication.

Next, we analyzed whether induction of autophagy upon Cx43 depletion was related to its involvement in signal transduction[29]. $Cx43^{-/-}$ cells displayed reduced ERK and AMPK phosphorylation and enhanced GSK3 phosphorylation, previously described to be conducive to autophagy repression[30–32], rather than to the autophagic activation observed in these cells (Supplementary Fig. 3e). The activity of the mTOR pathway, negative regulator of autophagy, and its down-regulation by rapamycin or serum removal were comparable in control and $Cx43^{-/-}$ cells (Supplementary Fig. 3f). Furthermore, both cell types displayed similar distribution and formation of ULK1-positive puncta (Supplementary Fig. 3g), in further support that autophagy upregulation was not a result of altered mTOR signaling. Therefore, our results support that autophagy upregulation was a primary consequence of the loss of the Cx43 protein rather than secondary to a reduction of its known cellular functions.

We next analyzed the impact of the phosphorylation state of $Cx43^{33}$ on its inhibitory effect on autophagy. Inhibition of PKA, PKC or ERK, described to phosphorylate $Cx43^{33}$, discretely enhanced autophagic activity but independently of the presence or not of Cx43 (Fig. 3c, d). In contrast, inhibition of Src lead to a robust induction of autophagy in control cells as described before[34], but failed to further enhance autophagy in $Cx43^{-/-}$ cells (Fig. 3c, d). The stimulatory effect of rapamycin on $Cx43^{-/-}$ cells supported that the lack of effect of the Src inhibitor was not due to autophagy saturation. Although the two described Src phosphorylation sites are located in its C-terminus (Tyr247 and Tyr265), overexpression of the C-terminus alone was insufficient to repress autophagy in $Cx43^{-/-}$ cells and it could not be pulled down with Atg16 (Fig. 3e, f), suggesting that either the membrane location and/or

other regions of this protein were required for autophagy inhibition. Expression of a GJ "functionally dead" C-terminus tagged Cx43 (Cx43-GFP) that localizes to the PM effectively reduced autophagy in these cells, further reinforcing that loss of GJ function was not behind the autophagy upregulation (Fig. 3e). A truncated version of GFP-Cx43 at residue 258 that lacks most of the C-terminus (ΔC) but preserves the proximal Src-phosphorylation site, repressed autophagy and could still be pulled down with Atg16 (Fig. 3e, g). However, the ability to repress autophagy was loss in a truncated Cx43 version only 13 residues shorter (truncate at residue 245) that lacks this proximal Src-phosphorylation site (Fig. 3e). In summary, these results support that the effect of Cx43 on autophagy does not depend on its role in GJ communication or signal transduction, but it requires the physical interaction of autophagy precursors, such as Atg16, with regions outside Cx43 C-terminus and a Src-dependent phosphorylation in the proximal tyrosine residue of the C-terminus.

Cx43 internalization abrogates its inhibitory effect on autophagy

To evaluate the consequences of physiological changes in the amount of Cx at the PM on autophagy, we induced acute internalization of GJ with either lindane (γ-hexachlorocyclohexane) or tamoxifen (Tx)[35, 36]. Both drugs under conditions that do not compromise cell viability (Supplementary Fig. 4a) led to the expected internalization of Cx43 (Supplementary Fig. 4b) as well as higher LC3-II steady-state levels, number of LC3-positive compartments and LC3 flux (Fig. 4a–d). Similar treatments in $Cx43^{-/-}$ cells did not further activate autophagy (Fig. 4d and Supplementary Fig. 4c show flux of exogenous or endogenous LC3, respectively).

Tx-induced internalization of Cx required active autophagy (Supplementary Fig. 4d, e), but this release of the Cx43 blockage of autophagy through its internalization may occur in response to specific stimuli, such as starvation but it could not be triggered by rapamycin (Supplementary Fig. 4f). Chemical-induced internalization of Cx43 coincided with an increase in the number of Atg16-positive pre-autophagic compartments (Fig. 4e, f) comparable to the one in Cx43-deficient cells (Fig. 4g, h). The internalized Cx43 colocalized with Atg16 vesicles both positive and negative for LC3 (Fig. 4f) but internalization led to reduced interaction between Atg16-Cx43 (Fig 4i) in further support that binding between both proteins occurs at the PM and that once in the pre-autophagosomal structures both proteins dissociate although they remain in the same compartment. All together, these results support that the presence of Cx43 at the PM is required for its inhibitory effect over autophagy and that degradation of this endogenous inhibitor through autophagy contributes to release its autophagic blockage.

Internalized Cx43 is targeted to recycling endosomes

We have previously shown that autophagy-induced internalization of Cx43 is mediated by clathrin in an Eps15-dependent manner[18], but the endocytic compartments[37] involved in this traffic are unknown. Since endosomal compartments contribute to the formation of pre-autophagosomal structures and are sites of confluence of Atg from different sources including PM[10, 11, 38], we analyzed the endocytic route followed by Cx43 upon autophagy-induced internalization.

Immunofluorescence analysis after serum deprivation or lindane treatment did not reveal significant colocalization of Cx43 with early (EEA1) or late (Rab9) endosomal markers and only discrete co-staining with Rab7, involved in endosome and autophagosome maturation[39] (Fig. 5a–c). Immunoblot analysis of purified Rab9-positive late endosomes demonstrated the presence of pre-autophagosome components in this fraction, such as Atg16 and LC3-II but almost complete absence of most Cx (Fig. 5d, e). Only during starvation, some Cx43 became visible in late endosomes (Fig. 5e) but at relatively low levels when compared to the amount in autophagosomes (Fig. 1a).

Cytosolic vesicles containing Cx43 internalized upon induction of autophagy were positive for transferrin (Fig. 5f–h), common marker of recycling endosomes, recently described as sites of arrival of autophagic precursors for autophagosome biogenesis[11, 33]. Interestingly, part of the Atg16 reaching this compartment has been shown to originate from the PM, suggesting that Cx43 and Atg16 travel together to recycle endosomes where they coincide with LC3 and additional autophagosome precursors.

Recruitment of Atg to Cx43-enriched plasma membrane regions upon autophagy induction

We next investigated if besides Atg16 other Atgs associated with Cx43. Immunoblot demonstrated the presence in isolated PMs of Atg16 along with multiple components of the class III phosphatidylinositol-3 kinase complex (PI3K) (initiation complex) both under fed and starvation conditions (Fig. 6a). The three main core proteins of this kinase complex, Vps34, Beclin-1 and Vps15 could be pulled down with Cx43 both in serum-supplemented cells and upon serum removal (Fig. 6b and Supplementary Fig. 5a). Rapamycin treatment (Supplementary Fig. 5b), Atg5-deficiency (Fig. 6c) or knock-down of Atg16 (Fig. 6d and Supplementary Fig. 5c) did not affect the PI3K-Cx43 interaction. The negative regulator of the Vps34 kinase activity, Rubicon[40, 41] was not detected in the Cx-Atg complex (Fig. 6b) whereas its positive regulator Atg14 was only retrieved in the Cx43 pull downs upon serum removal (Fig. 6b). In fact, Atg14 content was higher in PM fractions isolated during nutrient deprivation (Fig. 6a) and Atg14 could be detected at Cx43-enriched regions of the PM under these conditions (Fig. 6e, Supplementary Fig. 5d). Video microscopy and 3D reconstruction confirmed the arrival of Atg14 and its mobilization along GJ during the first hour of serum removal (Fig. 6f). Contrary to Cx43, Atg14 was no present in autophagosomes (Fig. 5d and Supplementary Fig. 5e) and did not undergo lysosomal degradation (Supplementary Fig. 5d).

The serum-dependent association of Atg14 with Cx43 could not be triggered by rapamycin (Supplementary Fig. 5b), was independent of the presence of Atg16 (Fig. 6d), was preserved during chemically-induced Cx43 internalization (Fig. 4i) and even if late steps of autophagosome formation were compromised (i.e. Atg5$^{-/-}$ cells; Fig. 6g). Although the proximal Src-phosphorylation site was required for the inhibitory effect of Cx43 on autophagy (Fig. 3e), its elimination was not sufficient to promote Atg14-Cx43 association under basal conditions (Supplementary Fig. 5f). PM association of the PI3K complex is independent of Atg16, Atg5 or Atg7, but we confirmed its dependence on Cx43. Both biochemical analysis of isolated PMs (Fig. 6h) and image-based procedures (Fig. 6i) demonstrated a drastic reduction in levels of PI3K components in the PM of Cx43-deficient

cells. In addition, contrary to the cytosolic redistribution of Atg14 observed in control cells upon serum removal, Atg14 remained confined in the Golgi under these conditions in Cx43-deficient cells (Supplementary Fig. 5g).

Arrival of Atg14 to the Cx-Atg complex coincides with an increase of PI3P (the phospholipid product of Vps34 detected using a fluorescent-tagged FYVE domain)[42] in the PM domains containing Cx43 (Fig. 6j). These findings are suggestive of autophagosome biogenesis from this PM location during starvation-induced autophagy.

Atg14 and Atg9 trigger Cx43 internalization and release its inhibitory effect on autophagy

Internalized Atg9 from the PM into the recycling endosome compartment, where it coincides with Atg16 to initiate autophagosome biogenesis, has been recently described[11]. We found that similar to Atg14, PM levels of Atg9 (Fig. 7a and Supplementary Fig. 6a) and its interaction with Cx43 (Fig. 7b) increased upon serum removal. Association of Atg9 with Cx43 was not disrupted, and in fact it was enhanced, if the later steps in autophagosome formation were inhibited (i.e. Atg7 knock-down is shown in Supplementary Fig. 6b), suggesting that the interaction of Atg9 with Cx43 occurs before autophagosome formation. Inhibition of the PI3K activity with 3-methlyadenine did not affect the association of Atg9 with Cx43 (Fig. 7c). Contrary to Atg14, PM arrival of Atg9 occurs independently of Cx43, and actually Cx43-deficient cells have higher Atg9 content in their PM (Fig. 7d and Supplementary Fig. 6c). Interestingly, interventions that prevent the internalization of Cx43 (i.e. Eps15 knock-down) increased the amount of Atg9 at PM (Fig. 7e) and bound to Cx43 (Supplementary Fig. 6d), suggesting that although recruitment of Atg9 to the PM does not require Cx43 (Fig. 7d), both proteins interact in this compartment prior to Cx43 internalization.

To further characterize the serum-dependent arrival of Atg14 and Atg9 to Cx43-Atg, we knocked them down separately (Supplementary Fig. 6e). Association of Atg14 and Atg9 with Cx43 was not interdependent, since Atg14 was still retrieved in the Cx43-pull downs in Atg9-deficient cells (Supplementary Fig. 6f) and Atg9 retained its serum-dependent association with Cx43 in Atg14-deficient cells (Supplementary Fig. 6g). However, depletion of either of them was sufficient to prevent serum-dependent (Fig. 7f, g) or chemically-induced (Fig. 7h and Supplementary Fig. 6h) internalization of Cx43 from the PM. We conclude that arrival of Atg14 and Atg9 to Cx43-enriched PM regions occurs independently but the temporal and spatial coincidence of both Atgs in these regions is required to trigger Cx43 internalization and the subsequent autophagic degradation of this endogenous autophagy inhibitor.

Conserved inhibitory effect of Cx on autophagy

Cx43 belongs to a family of transmembrane proteins with common structure but divergent intracytoplasmic loops and C-terminal tails[43] (Supplementary Fig. 7a). Since other Cx are also highly enriched in autophagosomes (Fig. 1a and Supplementary Fig. 1a) and undergo degradation by autophagy[18, 19], we analyzed the possible autophagy inhibitory effect of other Cx. Separate knock-down of Cx26, Cx32 or Cx43 present in mouse embryonic fibroblasts (MEFs) (Fig. 8a and Supplementary Fig. 7b) led in all cases to: i) increase in

LC3-fluorescent puncta, ii) higher LC3-II steady-state levels, iii) enhanced LC3-II flux by immunoblot and by the mCherry-GFP-LC3 reporter, iv) high number of autophagolysosomes by electron microscopy and v) higher rates of “in bulk” autophagy (total rates of long half-life protein degradation) and of selective autophagy (oleic acid induced macrolipophagy is shown) (Fig. 8b–e and Supplementary Fig. 7c–f).

As in the case of Cx43, both recombinant expressed (Supplementary Fig. 7g) and endogenous Cx26 and Cx32 (Fig. 8f) also interact with Atg16. Overall, these results support that the inhibitory effect of Cx43 on autophagy and its interplay with Atg involved in autophagosome biogenesis is shared by other members of the connexin family.

Discussion

In this work, we describe a constitutive inhibitory effect of PM Cx on autophagosome biogenesis that can be suppressed by internalization and degradation of Cx by autophagy. By degrading these negative regulators, cells might assure maximal activation of autophagy in response to nutritional stress.

The inhibitory effect of Cx43 on autophagy seems independent of its function in intercellular communication and signaling because (i) the impact on autophagy of GJ blockage and Cx absence are opposite, (ii) forms of Cx inactive for these other functions (i.e. N-terminus GFP-tagged Cx43[45]) still inhibit autophagy and (iii) the C-terminus of Cx, essential for these other functions, is not required for autophagy inhibition. We propose that Cx act as negative regulators of autophagy under basal conditions by sequestering the initiation complex PI3K in an inactive status at the PM and by trapping a pool of the pre-autophagosomal protein Atg16 in this compartment (Supplementary Fig. 8). The presence of this reservoir of pre-assembled but inactive autophagy initiation complexes bound to Cx at the PM may eliminate the need for *de novo* synthesis of Atgs to initiate autophagosome biogenesis in conditions such as nutritional starvation when protein synthesis is reduced. Activation of the nucleation kinase activity upon recruitment of Atg14 and the coincident arrival of Atg9 to this location trigger Cx internalization and release of its inhibitory effect. Although inhibition of PI3K did not prevent Cx binding to either of the autophagosome precursors, Atg16 and Atg9, it blocked the internalization of this complex, suggesting that phosphorylation of PM lipids in the proximity of the Cx-Atg complex could promote conformational changes in this complex required for its internalization and subsequent maturation of the pre-autophagosomal structures into autophagosomes. Future studies are required to determine if one of these conformational changes also prevent Src-mediated phosphorylation of Cx43, required to sustain its inhibitory effect on autophagy. The fact that this phosphorylation has been linked to GJ closing[45] opens the intriguing possibility that Cx43 not engaged in cellular communication but present at the PM are the ones involved in Atg sequestration in this compartment.

Although the presence of Cx in recycling endosomes could contribute to further recruitment of Atg precursors from different sources, we propose that Cx interacts with Atg16 and the PI3K complex at the PM before their trafficking to recycling endosomes as (i) we can detect these Atgs at Cx43-enriched regions of the PM, (ii) they remain at the PM when Cx

internalization is blocked and (iii) they are no longer visible at the PM of Cx-deficient cells. Atg9 that normally resides in small cytoplasmic vesicles[46], reaches the PM during starvation in a Cx- and PI3K-independent manner but it requires Cx for its internalization.

Although in our model we depict Atg16, Atg14/initiation complex and Atg9 all interacting with the same Cx complex (Supplementary Fig. 8), it is possible that each of these Atg binds to different molecules of Cx43 and that the ability of this structural membrane protein to multimerize contributes to bringing together the different parts of the autophagosome initiation complex. It is possible that Atg9 and Atg16 are part of Cx heterocomplexes and that disassembly of Cx during internalization may be responsible Atg9 and Atg16 segregating through different vesicles in their route from the PM to the recycling endosomes (Supplementary Fig. 8).

The identification of PM Cx as endogenous negative regulators of autophagy presents them now as possible targets to enhance autophagy activity under conditions when maximal activation of autophagy is needed.

Online Methods

Animals and cells

Adult (4–6 months) male Wistar rats and C57BL/6 mice (Charles River Laboratories) were used. Where indicated, animals were starved for 6h or 24h before organelle isolation by completely removing food but maintaining water supply *ad libitum*. $Cx43^{+/-}$ mice were generated as described before[47]. All animal procedures were conducted under an animal study protocol approved by the Institutional Animal Care and Use Committee of the Albert Einstein College of Medicine. Mouse embryonic fibroblasts (MEFs) from mice null for Atg5 ($Atg^{-/-}$) were a generous gift of Dr. N. Mizushima (U. Tokyo, Japan). Mouse osteoblasts (MOBs) from $Cx43^{-/-}$ mice were generated as described before[23]. Normal rat kidney (NRK) cells and HeLa cells were from the American Type Culture Collection. All cells were cultured in Dulbecco's Modified Eagle's Medium (Sigma) containing 10% FBS 50μg/ml penicillin, and 50μg/ml streptomycin at 37°C with 5% CO_2. Knock-out of the proteins of interest (Atg5 and Cx43) was tested periodically (each 2–3 months) during the study and representative immunoblots for the absence of the proteins are included in the manuscript. All the cells lines were tested for mycoplasma contamination using DNA staining protocol with Hoechst 33258 dye. Serum removal was performed by thoroughly washing the cells with Hanks' Balanced Salt Solution (Invitrogen) and placing them in serum-free medium. Where indicated, macroautophagy was inhibited by addition of 3-methyladenine (10mM) (Sigma) and lysosomal proteolysis was inhibited by addition of chloroquine (50μM) or with NH_4Cl (20mM) and leupeptin (100μM) (Fisher BioReagents). The fluorometric CellTiter-Blue Assay from Promega was used as method for assessing cell viability upon tamoxifen and lindane treatments.

Chemicals and plasmids

Sources of chemicals and antibodies were as described previously[3,6,9] and except where it stated differently they were used at dilution 1:1,000 (for immunoblot IB) and 1:200 (for immunofluorescence IF). The antibodies against Cx43 (#C6219; 1:2,000 IB), Cx32

(#C6344; 1:500 IB), flag (#F1804; 1:2,000 IF) and β-tubulin (#T8328) were from Sigma-Aldrich; against Vps34 (#382100; 1:500 IB), Cx43 (#138300 and #710700; 1:500 IB), Cx32 (#358900; 1:500 IB), and Cx26 (#335800 and #710500; 1:500 IB) from Invitrogen; against LAMP1 (#VAM-EN001) from Stressgen; against calnexin (#MA3-027; 1:10,000 IB) from Affinity Bioreagents; against GAPDH (#ab8245) and actin (#ab6276) from Abcam; against LC3 (#2775), ERK1/2 (#9101), P-ERK1/2 (#9102), mTOR (#2972), P-mTOR (Ser2448) (#2971), P-p70S6K (#9205), p70S6K (#9202), P-GSK3 (#9331), GSK3 (#5676), P-AMPK (#2531), AMPK (#2603) and Atg7 (#2631) from Cell Signaling Technology; against ULK1 (#NB110-74844), Atg9 (#NB100-56893;1:500 IB), Vps15 (#NBP1-304630), Eps15 (#NB110-74688), Atg5 (#NB110-53818) from Novus Biologicals; against Cx43 (#610061), e-cadherin (#610182), Beclin-1 (#612112; 1:2,000 IB), GM130 (#558712), EEA1 (#610456), BiP (#610987; 1:10,000 IB) and clathrin (#610499) from BD Biosciences, against LC3 (#M152-3 and #PM036), Atg16 (#PM040), Atg14 (#PD026) and Rubicon (#PD027) from MBL; against GABARAP (#sc-28938), Rab9 (#sc-28573) and Rab7 (#sc-10767; 1:500 IB) from Santa Cruz and against GRP94 (#SPA-850; 1:15,000 IB) from Assay Designs. The anti-GFP antibody peroxidase conjugated (#600-103-215) was from Rockland and the antibody against Na+/K+ ATPase was donated by Dr. W. J. Ball (University of Cincinnati, OH). The Atg16 constructs were generously donated by Dr. Rubinsztein (U. Cambridge, UK), GFP-Cx43 was a generous gift from Dr. Pereira (U. Coimbra, Portugal), and the C-terminus Cx43 tagged to flag and the mCherry-GFP-LC3 and pEGFP-Atg14 were from Addgene. SuperfolderGFP and EBFP2 plasmids were generously provided by the Fluorescent Protein Resource Center of Albert Einstein College of Medicine. N-terminal tagged full length Cx43 and ΔCT_{258} or ΔCT_{245} were inserted in the Sac1 linearized EGFP-C1 vector that contains the sequence for superfolderGFP or EBFP2 in place of the EGFP coding sequence using the following primers: N-terminal tagged Cx43 primers: common forward primer (CGGACTCAGATCTCGAGCTCAGATGGGTGACT GGAGTGCCTTG), full length Cx43 reverse primer (AGAATTCGAAGCTTGAGCTCT TAAATCTCCAGGTCATCAGGC), Δ CT_{258}-Cx43 reverse primer (AGAATTCGAAGCTTGAGC TCTTATGATGGGCTCAGTGGGCCAG) and ΔCT_{245} reverse primer AGAATTCGAAGCTTGAGCTCTTAGCTTCTTC CCTTCACGCGATCC). Cx43-sfGFP with the removed stop codon was inserted in the Sac1 linearized sfGFP-N1 vector using the following primers: forward (TCGACGGTACCGCGGGCCCGGGCACCAATG GGTGACTGGAG) and reverse (GGTGGCGACCGGTGGATCCCGGGCGGAAATCTCCA GGTCATCAG). sfGFP-ATG16 was constructed by inserting the mouse ATG16L1 variant 3 sequence (Addgene 24302) in the Sac1 linearized sfGFP-N1 vector using the following primers: forward (CGGACTCAGA TCTCGAGCTCAGATGTCGTCGGGCCTGCGC) and reverse (AGAATTCGAAGCTTGAGC TCTCAAGGCTGTGCCCACAGCAC). pEGFP-2xFYVE$_{Hrs}$ was donated by Dr. Jonathan M. Backer. Cx-Dendra2 construct were generously provided by Michael Davidson (Florida State University, FL). Tamoxifen, lindane and 18α glycyrrhetinic acid were from EMB Biosciences. Transferrin-594, *FAST* DiI, and secondary antibodies were from Life Technologies. The inhibitors of the kinase activity of PKC were from Promega, PKA from Enzo Life Science, ERK (U01256) from Cell Signaling and Src (AZD0530) from Selleck Chemicals.

Cell transfection and RNA interference

Cells were transfected with cDNA constructs using either Lipofectamine2000 or Optifect reagent (Invitrogen) according to manufacturer's instructions. For lentivirus-mediated shRNA transfer vector plasmids containing shRNA against Cx43, 32, 26 and Atg7, Atg14 and Eps15 were purchased from Sigma Mission Library and were against the following sequences: Cx26 (CCGGGAGAGATAAAGAACGAGTTTA); Cx32 (CCGGCTCACCTGAATACAAGCAGAA); Cx43 (CCGGCCCACCTTTGTGTCTTCCATA); Eps15 (CCGGCCTATGAGCATGGGATACAAA); Atg16 (CA ATGTGTAATGAGTGGACAT and AGCTTCAAATGATTTTGCA); Atg9A (CCACCGGCTTATCAAGTTTAT and GGCTTA TCAAGTTTATCTA); Atg14 (CCGTACACAAACAGCTTTCTA and GCTGAAGCAAACA ATATGTAA) and Atg7 (GATCCCCGCAGCTCATTGATAACCAT). Lentiviral particles were generated by co-transfection with the third-generation packaging constructs pMDLg/pRRE and pRSV-REV, and as envelope the G glycoprotein of the VSV (pMD2.G) into HEK293T cells as described before[44].

Immunostaining and image analysis

Indirect immunofluorescence was performed following conventional procedures. Briefly, cells were grown on coverslips, fixed in either cold methanol or 4% paraformaldehyde, blocked and permeabilized (1% BSA, 2% New born calf serum, 0.01% Triton X-100), and then incubated with the primary and corresponding fluorophore-conjugated secondary antibodies as described[48]. Except otherwise noted, all slides were mounted for microscopy using Fluoromount-G (SouthernBiotech) containing DAPI (4′,6-diamidino-2-phenylindole) to highlight the nucleus. Images were collected using either ApoTome.2 system in an Axiovert 200 fluorescence microscope (Carl Zeiss) equipped with a ×63 1.4 N.A. oil objective or a laser-scanning confocal microscope Leica SP5II AOBS (Leica) and prepared using Adobe Photoshop 6.0 software (Adobe Systems). For quantitative analysis, z-stack images of MEFs were merged in a single image, but in the case of MOB cells that are considerably flatter, a single image was taken at the section of the maximum nucleus diameter. The number of fluorescent cytosolic particles (puncta) per cell was determined using the Analyze Particles function of ImageJ (NIH) after applying a fixed threshold to all images. Percentage of colocalization was calculated using the JACoP plug-in in this software. All quantifications were done blindly. 3D reconstruction images were modeled as mixed rendering using the Inside4D module for AxioVision Rel. 4.8 after applying the Nyquist sampling criteria. Videomicroscopy and 3D reconstruction images were carried out in a Zeiss 510 LSCM microscope, 63x-Plan-Apochromat/1.40 Oil DIC objective, Dual-Channel, 405 and 489 nm laser illumination with 415–480 and 520–555 nm bandpass filters, respectively. All representative images include quantification in the same or next panel and the number of repetitions is indicated in the corresponding figure legends.

Autophagic measurements

Intracellular protein degradation was measured by metabolic labeling with [^{3}H]leucine (NENPerkinElmer Life Sciences) for 48h at 37°C and chase of the radiolabeled amino acids

released to the media at different times as described before[49]. Autophagic flux was measured by immunoblot as changes in levels of LC3-II upon inhibition of lysosomal proteolysis (net flux) and autophagosome formation as the increase in LC3-II levels at two consecutive times during lysosomal proteolysis inhibition[50]. Autophagosome content was evaluated as the number of fluorescent puncta after immunostaining with antibodies against endogenous LC3. Autophagic flux was also tested by transient transfection of the mCherry-GFP-LC3 plasmid. Quantification of the yellow and red puncta was performed by Green and Red Puncta Colocalization Macro for ImageJ (D. J. Swiwarski modified by R.K. Dagda).

Electron microscopy

Cultured cells and liver sections were fixed in 4% paraformaldehyde/0.1% glutaraldehyde in 100mM sodium cacodylate, pH 7.43, dehydrated and embedded in LR-White resin (LADD Research Industries). All grids were viewed on a JEOL 100CX II transmission electron microscope at 80kV. Morphometric analysis of transmitted electron micrographs was done blinded using ImageJ (NIH). Autophagic vacuoles were identified using standard criteria[44] and were catalogued as autophagosomes or autophagolysosomes if they meet two or more for the following criteria: for autophagosomes they should have double membrane (completely or partially visible), absence of ribosomes in the outer membrane, luminal density comparable to the surrounding cytosol and identifiable organelles or regions of organelles in their lumen; for autophagolysosomes they should have similar size but less than 40% of membrane visible as double, luminal density lower than surrounding cytosol and luminal material no recognizable as specific organelles and/or amorphous material. Primary and secondary lysosomes (identified as single membrane vesicles of higher density and smaller average diameter) were excluded from the quantification. The term autophagic vacuole was used for those instances in which differentiation between autophagosomes and autophagolysosomes was not possible. Annotated micrographs were independently reviewed by two people and the average of their scoring was used for each micrograph. All representative images include quantification in the same figure or as supplementary figure and the number of repetitions is indicated in the corresponding figure legends.

Subcellular fractions

Plasma membrane, ER and Golgi fractions were isolated from rat liver using procedures described previously[51]. Autophagic vacuoles were isolated from mouse liver using discontinuous metrizamide density gradient as described previously[52]. Endosomal isolation was carried out as previously described[53].

Immunoblot and immunoprecipitation

Cell lysates were prepared by solubilization in RIPA buffer (1% Triton-X 100, 1% sodium deoxycholate, 0.1% SDS, 0.15M NaCl, 0.01M sodium phosphate, pH 7.2) containing protease and phosphatase inhibitors. The solubilized fraction was recovered in the supernatant after centrifugation at 12,000g for 30min, and protein concentration was measured by the Lowry method using bovine serum albumin (BSA) as a standard. Co-immunoprecipitation was done from cellular extracts solubilized in lysis buffer (190mM NaCl, 50mM Tris-HCl, 6mM EDTA, 1% Triton X-100, pH 8.3) as described[18]. After SDS-PAGE and immunoblotting, the proteins recognized by the specific antibodies were

visualized by chemiluminescence methods (Western Lightning; PerkinElmer) using peroxidase-conjugated secondary antibodies. Membranes were developed using the LAS-3000 Imaging System (Fujifilm) and densitometric quantification was performed in unsaturated images using ImageJ (NIH). To avoid interference of the IgG signal in the immunoprecipitates whenever possible pulldowns and immunoblots for the same protein were performed using different species antibodies. Thus, Cx were immunoprecipitated using mouse monoclonal antibodies and immunoblot of these fractions developed using rabbit polyclonal antibodies. Reblotting for proteins of different molecular weight was performed without stripping to minimize epitope damage. All representative images of immunoblot include quantification in the same or next panel or for those cases in which quantification is not required the number of repetitions is indicated in the corresponding figure legends.

Statistical analysis and determination of sample size

All numerical results are reported as mean +s.e.m and represent data from a minimum of three independent experiments. GraphPad InStat software (GraphPad) was used for analysis of statistical significance. If no indicated otherwise in the legend to the figures two-tailed Student's *t* test for unpaired data was used to evaluate single comparisons between different experimental groups. As indicated in the legends to the figures, for multiple comparisons a one-way analysis of variance followed by Bonferroni *post hoc* test was used. Differences were considered statistically significant for a value of $p < 0.05$. All the experiments were performed at least 3 times and often in duplicate or triplicate in the same experiments. In all instances "n" refers to individual experiments. In the case of studies with animals, sample size was calculated as follows: 1) For the morphometric studies with livers of wild-type and heterozygous Cx43 mouse models, power analysis was performed to decide the number of animals required using as reference the previous differences in numbers of autophagosomes and autophagolysosomes that we have found in conditions such as aging or in models manipulating other autophagic pathways. Power analysis with the sample size utilized and a two-sided Type 1 error rate of 5% predicted >80% power to detect effects of 1.2 or greater in number, average size and ratio of different types of autophagic vacuoles; 2) for the studies of isolation of lysosomes and cell fractionation (including plasma membrane) the number of animal for preparation has been determined based on the average values of enrichment and recovery for the specific fraction using endogenous markers for each compartment. Power analysis with the sample size utilized and a two-sided Type 1 error rate of 5% predicted >80% power to detect effects of 2.1 or greater in levels of lysosomal components. None of the animals were excluded from the study and inclusion in a group was solely based on genotyping. There was not randomization as animals were not subjected to any specific treatment and group allocation was based on genotype. For those experiments in which an estimate of variation was possible based on previous studies or published work by others we have confirmed that the variance is similar between the control and experimental groups compared. For those instances in which previous information was not available (i.e. changes in autophagy markers in Cx deficient cells) we have compared with other conditions in which changes in cellular components (i.e. primary cilia) resulted in changes in autophagy.

Supplementary Material

Refer to Web version on PubMed Central for supplementary material.

Acknowledgments

We thank Dr. Mizushima for providing the Atg5$^{-/-}$ MEFs, Dr. Mia M. Thi for the immortalized wild type and Cx43$^{-/-}$ osteoblasts cell lines, Antonio Diaz-Carretero for technical assistance on DNA preparations and cell culture and Dr. Kaushik and Dr. Hutten for critically reviewing this manuscript. This work was supported by grants NIH/NIA AG031782, AG038072 and DK041018 and the generous support of Robert and Renee Belfer.

References

1. Yang Z, Klionsky DJ. Mammalian autophagy: core molecular machinery and signaling regulation. Curr Opin Cell Biol. 2010; 22:124–131. [PubMed: 20034776]
2. Mizushima N, Levine B, Cuervo AM, Klionsky DJ. Autophagy fights disease through cellular self-digestion. Nature. 2008; 451:1069–1075. [PubMed: 18305538]
3. Levine B, Mizushima N, Virgin HW. Autophagy in immunity and inflammation. Nature. 2011; 469:323–335. [PubMed: 21248839]
4. Mizushima N, Yoshimori T, Ohsumi Y. The role of Atg proteins in autophagosome formation. Annu Rev Cell Dev Biol. 2011; 27:107–132. [PubMed: 21801009]
5. Axe EL, et al. Autophagosome formation from membrane compartments enriched in phosphatidylinositol 3-phosphate and dynamically connected to the endoplasmic reticulum. J Cell Biol. 2008; 182:685–701. [PubMed: 18725538]
6. English L, et al. Autophagy enhances the presentation of endogenous viral antigens on MHC class I molecules during HSV-1 infection. Nat Immunol. 2009; 10:480–487. [PubMed: 19305394]
7. Hailey DW, et al. Mitochondria supply membranes for autophagosome biogenesis during starvation. Cell. 2010; 141:656–667. [PubMed: 20478256]
8. Ravikumar B, Moreau K, Jahreiss L, Puri C, Rubinsztein D. Plasma membrane contributes to the formation of pre-autophagosomal structures. Nat Cell Biol. 2010; 12:747–757. [PubMed: 20639872]
9. van der Vaart A, Griffith J, Reggiori F. Exit from the Golgi is required for the expansion of the autophagosomal phagophore in yeast Saccharomyces cerevisiae. Mol Biol Cell. 2010; 21:2270–2284. [PubMed: 20444982]
10. Knaevelsrud H, et al. Membrane remodeling by the PX-BAR protein SNX18 promotes autophagosome formation. J Cell Biol. 2013; 202:331–349. [PubMed: 23878278]
11. Puri C, Renna M, Bento CF, Moreau K, Rubinsztein DC. Diverse autophagosome membrane sources coalesce in recycling endosomes. Cell. 2013; 154:1285–1299. [PubMed: 24034251]
12. Kim J, et al. Differential regulation of distinct Vps34 complexes by AMPK in nutrient stress and autophagy. Cell. 2013; 152:290–303. [PubMed: 23332761]
13. Reggiori F, Tooze SA. Autophagy regulation through Atg9 traffic. J Cell Biol. 2012; 198:151–153. [PubMed: 22826119]
14. Mizushima N. The role of the Atg1/ULK1 complex in autophagy regulation. Curr Opin Cell Biol. 2010; 22:132–139. [PubMed: 20056399]
15. Suzuki K, Ohsumi Y. Current knowledge of the pre-autophagosomal structure (PAS). FEBS Lett. 2010; 584:1280–1286. [PubMed: 20138172]
16. Sanjuan MA, et al. Toll-like receptor signalling in macrophages links the autophagy pathway to phagocytosis. Nature. 2007; 450:1253–1257. [PubMed: 18097414]
17. Rowland AM, Richmond JE, Olsen JG, Hall DH, Bamber BA. Presynaptic terminals independently regulate synaptic clustering and autophagy of GABAA receptors in Caenorhabditis elegans. J Neurosci. 2006; 26:1711–1720. [PubMed: 16467519]
18. Bejarano E, et al. Autophagy modulates dynamics of connexins at the plasma membrane in a ubiquitin-dependent manner. Mol Biol Cell. 2012; 23:2156–2169. [PubMed: 22496425]

19. Lichtenstein A, Minogue PJ, Beyer EC, Berthoud VM. Autophagy: a pathway that contributes to connexin degradation. J Cell Sci. 2011; 124:910–920. [PubMed: 21378309]
20. Hesketh GG, et al. Ultrastructure and regulation of lateralized connexin43 in the failing heart. Circ Res. 2010; 106:1153–1163. [PubMed: 20167932]
21. Fong JT, et al. Internalized gap junctions are degraded by autophagy. Autophagy. 2012; 8:794–811. [PubMed: 22635056]
22. Girao H, Catarino S, Pereira P. Eps15 interacts with ubiquitinated Cx43 and mediates its internalization. Exp Cell Res. 2009; 315:3587–3597. [PubMed: 19835873]
23. Thi MM, Urban-Maldonado M, Spray DC, Suadicani SO. Characterization of hTERT-immortalized osteoblast cell lines generated from wild-type and connexin43-null mouse calvaria. Am J Physiol Cell Physiol. 2010; 299:C994–C1006. [PubMed: 20686067]
24. Weidberg H, et al. LC3 and GATE-16/GABARAP subfamilies are both essential yet act differently in autophagosome biogenesis. EMBO J. 2010; 29:1792–1802. [PubMed: 20418806]
25. Klionsky DJ, et al. Guidelines for the use and interpretation of assays for monitoring autophagy. Autophagy. 2012; 8:445–544. [PubMed: 22966490]
26. Kimura S, Noda T, Yoshimori T. Dissection of the autophagosome maturation process by a novel reporter protein, tandem fluorescent-tagged LC3. Autophagy. 2007; 3:452–460. [PubMed: 17534139]
27. Shah US, Murray SA. Bimodal inhibition of connexin 43 gap junctions decreases ACTH-induced steroidogenesis and increases bovine adrenal cell population growth. The Journal of endocrinology. 2001; 171:199–208. [PubMed: 11572804]
28. Goldberg GS, et al. Evidence that disruption of connexon particle arrangements in gap junction plaques is associated with inhibition of gap junctional communication by a glycyrrhetinic acid derivative. Exp Cell Res. 1996; 222:48–53. [PubMed: 8549672]
29. Dbouk HA, Mroue RM, El-Sabban ME, Talhouk RS. Connexins: a myriad of functions extending beyond assembly of gap junction channels. Cell communication and signaling : CCS. 2009; 7:4. [PubMed: 19284610]
30. Turner MS, et al. Reversible connexin 43 dephosphorylation during hypoxia and reoxygenation is linked to cellular ATP levels. Circ Res. 2004; 95:726–733. [PubMed: 15358666]
31. Mureli S, et al. Mesenchymal stem cells improve cardiac conduction by upregulation of connexin 43 through paracrine signaling. Am J Physiol Heart Circ Physiol. 2013; 304:H600–609. [PubMed: 23241322]
32. Plotkin LI, Manolagas SC, Bellido T. Transduction of cell survival signals by connexin-43 hemichannels. J Biol Chem. 2002; 277:8648–8657. [PubMed: 11741942]
33. Johnstone SR, Billaud M, Lohman AW, Taddeo EP, Isakson BE. Posttranslational modifications in connexins and pannexins. J Membr Biol. 2012; 245:319–332. [PubMed: 22739962]
34. Wu Z, et al. Autophagy Blockade Sensitizes Prostate Cancer Cells towards Src Family Kinase Inhibitors. Genes & cancer. 2010; 1:40–49. [PubMed: 20811583]
35. Dahm L, Klugmann F, Gonzalez-Algaba A, Reuss B. Tamoxifen and raloxifene modulate gap junction coupling during early phases of retinoic acid-dependent neuronal differentiation of NTera2/D1 cells. Cell biology and toxicology. 2010; 26:579–591. [PubMed: 20437090]
36. Guan X, Ruch RJ. Gap junction endocytosis and lysosomal degradation of connexin43-P2 in WB-F344 rat liver epithelial cells treated with DDT and lindane. Carcinogenesis. 1996; 17:1791–1798. [PubMed: 8824497]
37. Johnson KE, et al. Phosphorylation on Ser-279 and Ser-282 of connexin43 regulates endocytosis and gap junction assembly in pancreatic cancer cells. Mol Biol Cell. 2013; 24:715–733. [PubMed: 23363606]
38. Longatti A, et al. TBC1D14 regulates autophagosome formation via Rab11- and ULK1-positive recycling endosomes. J Cell Biol. 2012; 197:659–675. [PubMed: 22613832]
39. Jager S, et al. Role for Rab7 in maturation of late autophagic vacuoles. J Cell Sci. 2004; 117:4837–4848. [PubMed: 15340014]
40. Zhong Y, et al. Distinct regulation of autophagic activity by Atg14L and Rubicon associated with Beclin 1-phosphatidylinositol-3-kinase complex. Nat Cell Biol. 2009; 11:468–476. [PubMed: 19270693]

41. Matsunaga K, et al. Two Beclin 1-binding proteins, Atg14L and Rubicon, reciprocally regulate autophagy at different stages. Nat Cell Biol. 2009; 11:385–396. [PubMed: 19270696]
42. Gillooly DJ, et al. Localization of phosphatidylinositol 3-phosphate in yeast and mammalian cells. Embo J. 2000; 19:4577–4588. [PubMed: 10970851]
43. Cruciani V, Mikalsen SO. The vertebrate connexin family. Cell Mol Life Sci. 2006; 63:1125–1140. [PubMed: 16568237]
44. Singh R, et al. Autophagy regulates lipid metabolism. Nature. 2009; 458:1131–1135. [PubMed: 19339967]
45. Lampe PD, Lau AF. The effects of connexin phosphorylation on gap junctional communication. Int J Biochem Cell Biol. 2004; 36:1171–1186. [PubMed: 15109565]
46. Yamamoto H, et al. Atg9 vesicles are an important membrane source during early steps of autophagosome formation. J Cell Biol. 2012; 198:219–233. [PubMed: 22826123]
47. Reaume AG, et al. Cardiac malformation in neonatal mice lacking connexin43. Science. 1995; 267:1831–1834. [PubMed: 7892609]
48. Kaushik S, Cuervo AM. Methods to monitor chaperone-mediated autophagy. Methods Enzymol. 2009; 452:297–324. [PubMed: 19200890]
49. Auteri JS, Okada A, Bochaki V, Dice JF. Regulation of intracellular protein degradation in IMR-90 human diploid fibroblasts. J Cell Physiol. 1983; 115:159–166. [PubMed: 6302104]
50. Tanida I, Minematsu-Ikeguchi N, Ueno T, Kominami E. Lysosomal Turnover, but Not a Cellular Level, of Endogenous LC3 is a Marker for Autophagy. Autophagy. 2005; 1:84–91. [PubMed: 16874052]
51. Slusarewicz P, Nilsson T, Hui N, Watson R, Warren G. Isolation of a matrix that binds medial Golgi enzymes. J Cell Biol. 1994; 124:405–413. [PubMed: 8106542]
52. Marzella L, Ahlberg J, Glaumann H. Isolation of autophagic vacuoles from rat liver: morphological and biochemical characterization. J Cell Biol. 1982; 93:144–154. [PubMed: 7068752]
53. Castellino F, Germain RN. Extensive trafficking of MHC class II-invariant chain complexes in the endocytic pathway and appearance of peptide-loaded class II in multiple compartments. Immunity. 1995; 2:73–88. [PubMed: 7600303]

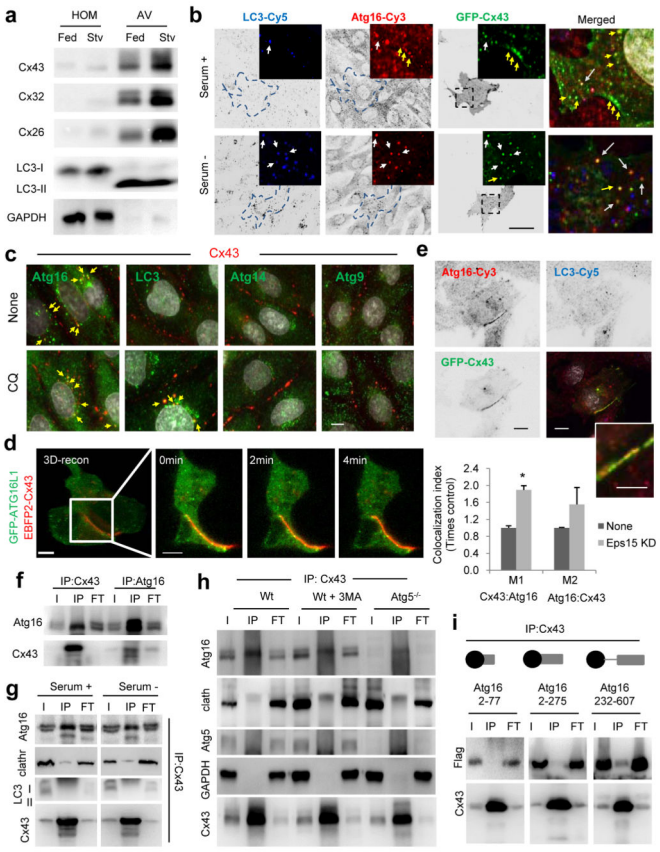

Figure 1. Atg16 associates with Cx43 in an early step of autophagosome biogenesis

(**a**) Immunoblot for the indicated Cx of homogenates and autophagic vacuoles (AV) isolated from fed or 6h starved (Stv) mice. Quantification of enrichment is shown in Supplementary Fig. 1a. (**b**) Immunofluorescence for LC3 and Atg16 in NRK cells expressing GFP-Cx43 maintained in the presence or absence of serum for 4h. Single channels are shown in reverse black and white and magnification of single and merged images are shown in color. Arrows: colocalization of Atg16/Cx43 (yellow) or Atg16/Cx43/LC3 (white). Quantification is shown in Supplementary Fig. 1c. (**c**) Immunofluorescence for the indicated endogenous proteins in NRK cells maintained in serum-supplemented media without additions (None) or treated with chloroquine (CQ) for 4h. Full fields are shown in Supplementary Fig. 1d. (**d**) Maximum projection confocal microscopy 3D reconstruction (left) followed by a single plane time-lapse acquisition of the region outlined by the white square in HeLa cells expressing EBFP2-Cx43 (pseudocolored in red) and sfGFP-ATG16. (**e**) Immunofluorescence for LC3 and Atg16 in NRK cells expressing GFP-Cx43 but knocked down for Eps15. Single channels are shown in reverse black and white and merged images in color. Inset shows higher magnification. *Bottom:* Quantification of colocalization between Atg16 and Cx43 (n=3 wells, 4 independent experiments, >20 cells per experiment). Values are mean+s.e.m. (*) p <0.05. (**f, g**) Immunoblot for the indicated proteins of immunoprecipitates (IP) of endogenous Cx43 and Atg16 from mouse embryonic fibroblasts (MEF) wild type cells maintained in the presence (f, g) or absence of serum (4h) (g). I: input; FT: flow through. (**h**) Immunoblot for the indicated proteins of immunoprecipitates

(IP) of endogenous Cx43 from MEFs wild type untreated (Wt), upon incubation with 3-methyladenine (3MA) or in MEFs from Atg5 null mice ($Atg5^{-/-}$). (**i**) Immunoblot for flag and Cx43 of immunoprecipitates (IP) of endogenous Cx43 in Wt MEFs transfected with the indicated flag-tagged constructs of truncated Atg16. GAPDH, LC3 and Atg5 are show as negative controls for IP. All values are mean+s.e.m. Nuclei are highlighted with DAPI. Bars: 5 μm. Uncropped images of blots are shown in Supplementary Fig. 9.

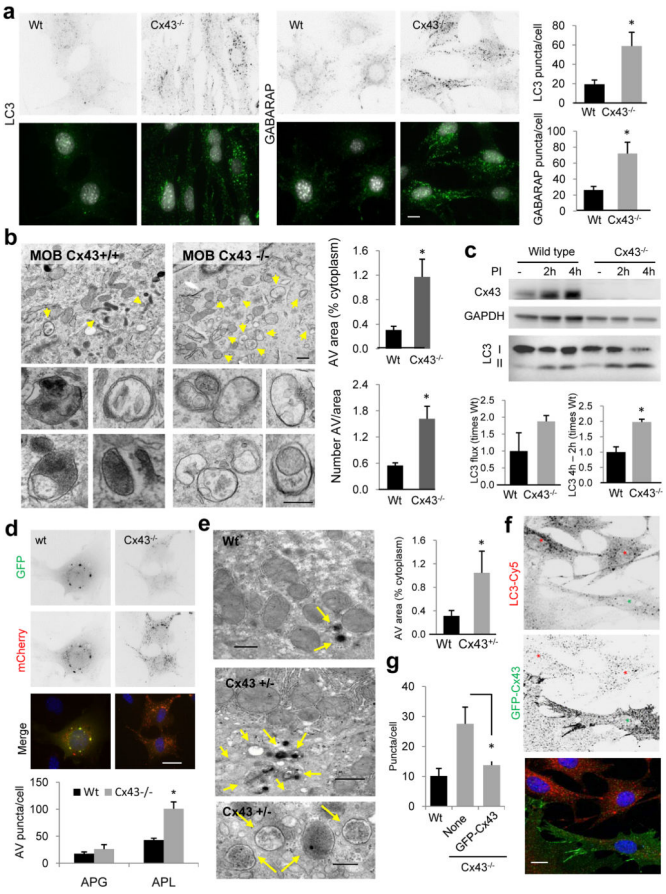

Figure 2. Autophagy is highly upregulated in cells from Cx43 knock-out mice

(**a**) Immunostaining for LC3 and GABARAP in mouse osteoblasts (MOB) from wild type (Wt) or Cx43 null mice ($Cx43^{-/-}$) grown in serum-supplemented media. Reverse black and white channels (top) and color images (bottom). *Right:* Average number of LC3 and GABARAP puncta per cell (n=3 wells, 3 independent experiments, >50 cells per experiment). (**b**) Electron micrographs of Wt and $Cx43^{-/-}$ MOB grown in serum-supplemented media. Yellow arrows: autophagic vacuoles. Insets: autophagic vacuoles (AV) at higher magnification. *Right:* Percentage of cytoplasm area occupied by AV (top) and number of AV per area (bottom) (n=3 mice, >10 micrographs per mice). (**c**) Immunoblot for LC3 of the same cells grown in serum-supplemented media untreated or treated with lysosomal protease inhibitors (PI) for 2 or 4h. Top: representative immunoblot. GAPDH is shown as loading control. Bottom: LC3 flux (left) and increase in LC3-II during lysosomal inhibition (right) (n= 3 independent experiments). (**d**) Representative images of the same cells transfected with the mCherry-GFP-LC3 tandem reporter and grown in serum-supplemented media. Single channel images (inverted black and white) and merged images (color). *Bottom*: Number of vesicles positive for GFP and mCherry (autophagosomes; APG) and only for mCherry (autophagolysosomes; APL) (n=4 wells, 4 independent experiments, >30 cells per experiment). (**e**) Electron micrographs of livers from Wt and $Cx43^{+/-}$ mice. Arrows indicate AV. *Right*: Percentage of cytosolic area occupied by AVs (n=3 mice, >10 micrographs per mice). (**f**) Immunofluorescence for LC3 in $Cx43^{-/-}$ MOBs expressing GFP-

tagged full-length Cx43. Single channels (inverted black and white) and merged channels (color). Asterisks: transfected (green) and untransfected (red) cells. (**g**) LC3-positive puncta per cell in the indicated cells (n=3 wells, 3 independent experiments, >50 cells per experiment). All values are mean+s.e.m. and differences with Wt were significant for (*) $p<0.01$. Nuclei are highlighted with DAPI. Bars: 5 μm in fluorescence images; 1 μm and 0.1 μm in top panels and inserts of b and e. Uncropped images of blots are shown in Supplementary Fig. 9

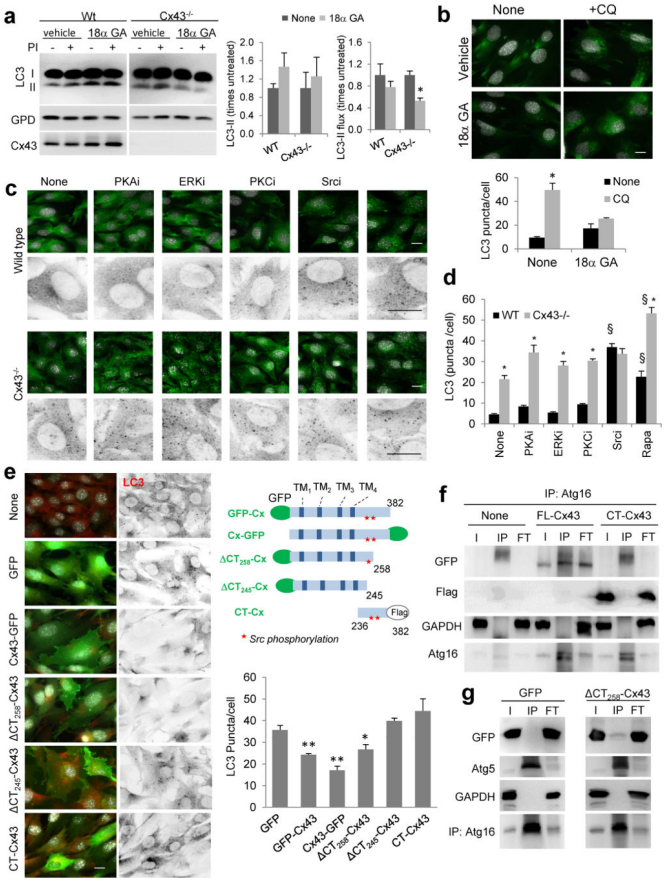

Figure 3. Cx43 domains responsible for the inhibitory effect over macroautophagy

(**a**) Immunoblot for LC3 in MOB from wild type (Wt) or Cx43 null mice ($Cx43^{-/-}$) treated with vehicle or with 18α glycyrrhetinic acid (18α GA). Glyceraldehyde-3-dehydrogenae (GPD) is shown as loading control. Levels of LC3-II (left) and LC3-II flux (right) (n= 3 independent experiments). (**b**) Immunofluorescence for LC3 in MOB cells treated with vehicle or 18α GA. Where indicated, chloroquine (CQ) was added to block lysosomal degradation. Bottom: Quantification of the average number of LC3-positive puncta per cell (n=3 wells, 3 independent experiments, >30 cells per experiment). (**c**) Immunofluorescence for LC3 in Wt or $Cx43^{-/-}$ MOBs cells treated with the indicated kinase inhibitors for 2 hours. Insets: Higher magnification images in inverted black and white. (**d**) Endogenous LC3 puncta in the same cells shown in c (n=3 wells, 3 independent experiments, >50 cells per experiment). *, differences with Wt and §, differences with untreated. **(e**) LC3 puncta in $Cx43^{-/-}$ MOBs transfected with constructs coding for different forms of Cx43 (full length, CT, ΔCT_{258} or ΔCT_{245}) tagged as indicated in the scheme. *Left:* Representative images. Merged fields (left) and LC3 channel in reverse black and white (right) are shown (images of GFP-Cx43 are shown in Fig. 2f). *Right:* Quantification of the average number of LC3 puncta per cell (n=3 wells, 3 independent experiments, >50 cells per experiment). (**f, g**) Immunoblot for the indicated proteins of the immunoprecipitates (IP) of Atg16 from MEFs transfected with GFP-tagged full length (FL-) Cx43 or flag tagged C-terminus (CT-) Cx43 (**f**) or ΔCT_{258}-Cx43 (**g**) I: input; FT: flow through. GAPDH and GFP alone were used as

negative controls for IP and Atg5 as positive control. All values are mean+s.e.m. Differences with control were significant for (*, §) $p<0.01$. Bars: 5 μm. Uncropped images of blots are shown in Supplementary Fig. 9.

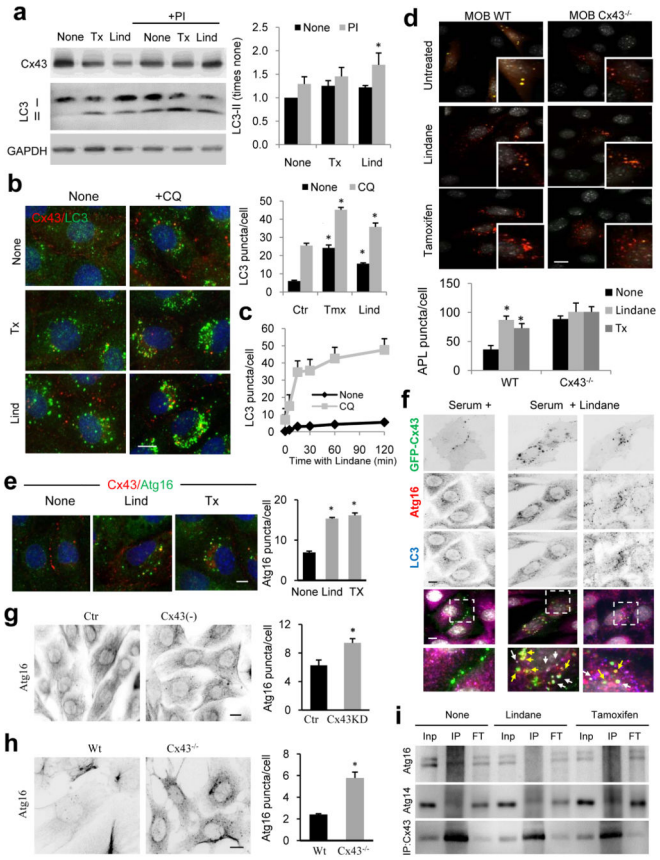

Figure 4. Cx43 internalization triggers mobilization of pre-autophagosomal structures from the plasma membrane and autophagosome biogenesis

(**a**) Immunoblots for the indicated proteins in mouse embryonic fibroblasts (MEFs) treated with tamoxifen (Tx) or lindane (Lnd) in the absence or presence of lysosomal protease inhibitors (PI). Right: Changes in LC3-II levels relative to those detected in untreated cells (n=4 independent experiments). (**b**) Immunofluorescence for Cx43 and LC3 in NRK cells treated as in a in the presence or absence of chloroquine (CQ) for 3h. *Right*: Quantification of the average number of LC3-positive puncta per cell (n= 3 wells, 3 independent experiments, >30 cells per experiment). (**c**) Time course of changes in the average LC3-positive puncta per cell after addition of Lnd to control NRK cells. (**d**) Fluorescence images of Wt or Cx43$^{-/-}$ MOBs transfected with mCherry-GFP-LC3 and incubated or not with Tx or Lnd. *Bottom:* Quantification of autophagolysosomes (n= 3 wells, 3 independent experiments, >50 cells per experiment). (**e**) Immunostaining for Atg16 and Cx43 in MEFs treated with the indicated compounds. Representative images as merged channels are shown. *Right:* quantification of the average of cytosolic Atg16-positive puncta per cell (n= 3 wells, 3 independent experiments, >30 cells per experiment). (**f**) Immunofluorescence for LC3 and Atg16 in NRK cells expressing GFP-Cx43 treated with Lnd and untreated. Single channel images in inverse black and white and merged color images are shown. Boxed areas are shown at higher magnification. Arrows: double (yellow) and triple (white) colocalization. (**g, h**) Immunostaining for Atg16 in Cx43 knocked down (−) (**g**) or knocked out ($^{-/-}$) (**h**) cells. *Right*: quantification of the average of cytosolic Atg16 positive puncta per cell (n= 3

wells, 3 independent experiments, >50 cells per experiment). (**i**) Immunoblot for Atg16 and Atg14 in immunoprecipitates (IP) of endogenous Cx43 from MEFs wild type cells maintained in the absence of serum (4h) or incubated in presence of Tx or Lind. I: input; FT: flow through. All values are mean+s.e.m and differences with untreated cells are significant for (*) $p<0.01$. Bars: 5 μm. Uncropped images of blots are shown in Supplementary Fig. 9.

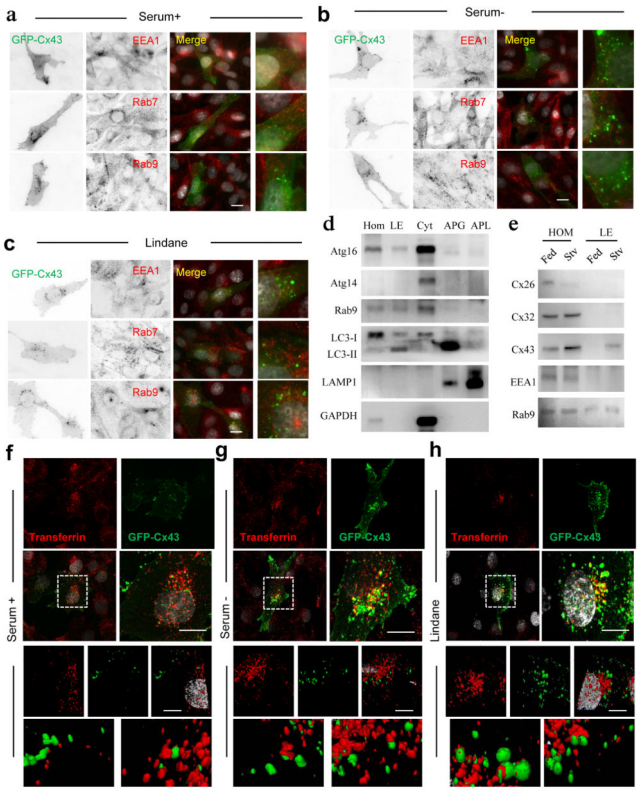

Figure 5. Internalized Cx43 is targeted to recycling endosomes during serum deprivation

(**a–c**) Immunofluorescence for the indicated endosomal markers in NRK cells expressing GFP-Cx43 maintained in presence of serum **(a)**, absence of serum (**b**) or treated with lindane (**c**). Single black and white inverted channels, merged channels and higher magnification insets are shown. (**d**) Immunoblots for indicated proteins in isolated fractions from starved mouse liver HOM: homogenate; LE: late endosomes; CYT: cytosol; APG: autophagosomes; APL: autophagolysosomes. (**e**) Immunoblots for different connexins in homogenates and late endosomes isolated from fed and 6h starved mice. (**f–h**) Fluorescence images of NRK cells expressing GFP-Cx43 maintained in presence of serum **(f)**, absence of serum (**g**) or treated with lindane (**h**) and incubated with Alexa594-transferrin for 15 minutes before fixation. *Top:* single and merged channels and boxed area at higher magnification. *Bottom:* 3D reconstructions and higher magnification details of the boxed areas. Nuclei are highlighted with DAPI. Bars: 5 μm. Uncropped images of blots are shown in Supplementary Fig. 9.

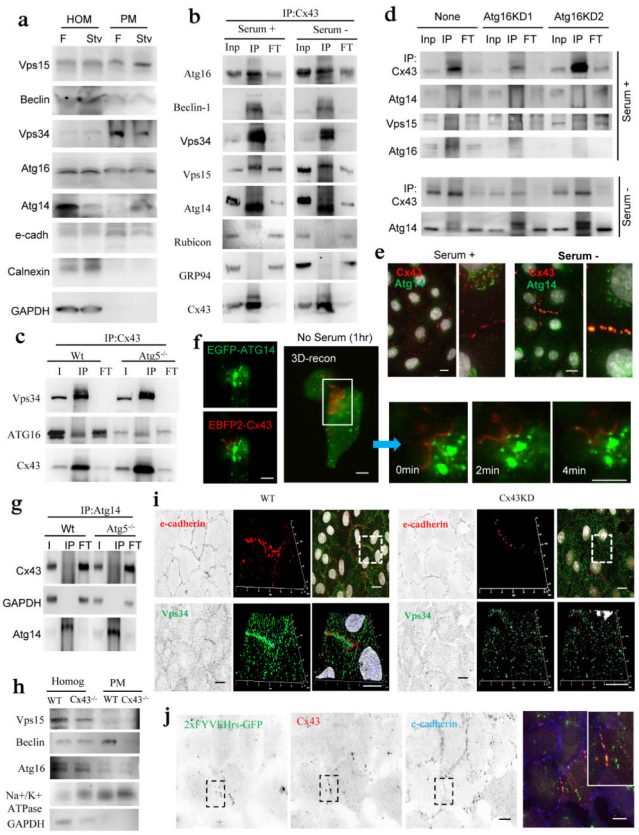

Figure 6. Atg14 is recruited to Cx43-enriched plasma membrane regions during nutritional deprivation

(**a**) Immunoblot for the indicated proteins in homogenates and purified plasma membrane from fed (F) and 24 h starved mice (Stv). Starvation-induced changes in the PM content relative to fed levels were as follows: Vps15 (1.2+0.2), Beclin-1 (0.7+0.5), Vps34 (0.9+0.1), Atg16 (1.1+0.3), Atg14 (2.5+0.2) and only Atg14 were significant for $p<0.01$. (**b**) Immunoblot of Cx43 immunoprecipitates (IP) in mouse embryonic fibroblasts (MEFs) maintained in the presence or absence of serum. I: input; FT: flow through. GAPDH is shown as negative control for IP. (**c**) Immunoblot of Cx43 IP in MEFs from Wt or $Atg5^{-/-}$ mice grown in serum-supplemented media. (**d**) Immunoblot of Cx43 IP in Wt or Atg16 knockdowns (KD) MEFs maintained in the presence/ absence of serum for 4h. (**e**) Co-staining for Atg14 and Cx43 in NRK cells maintained in presence/absence of serum. Merged channels are shown and single channels and broad field images are shown in Supplementary Fig. 5d. Insets: higher magnification. (**f**) Maximum intensity confocal microscopy 3D reconstruction in HeLa cells expressing EBFP2-Cx43 (pseudocolored in red) and EGFP-ATG14 followed by a single-plane time-lapse acquisition of the boxed area; cells were incubated in serum-deprived medium for 1h before imaging. (**g**) Immunoblot of Atg14 IP in Wt or $Atg5^{-/-}$ MEFs maintained in the presence of serum. (**h**) Immunoblot in total homogenates and plasma membrane (PM) purified from Wt or $Cx43^{-/-}$ mice. (**i**) Immunofluorescence for e-cadherin and Vps34 in NRK cells wild-type (Wt) or knocked down (−) for Cx43. Single channel and merge (left) and Z-stack surface reconstruction and higher magnification of the boxed region (right). (**j**) Immunostaining for Cx43 and e-

cadherin in NRK cells expressing a tandem FYVE domain (2xFYVE) tagged to GFP and maintained in serum-free media for 4h. Single channels (inverted black and white) and the merged image of the boxed area (color). Inset: higher magnification image. Bars: 5 μm. Uncropped images of blots are shown in Supplementary Fig. 9.

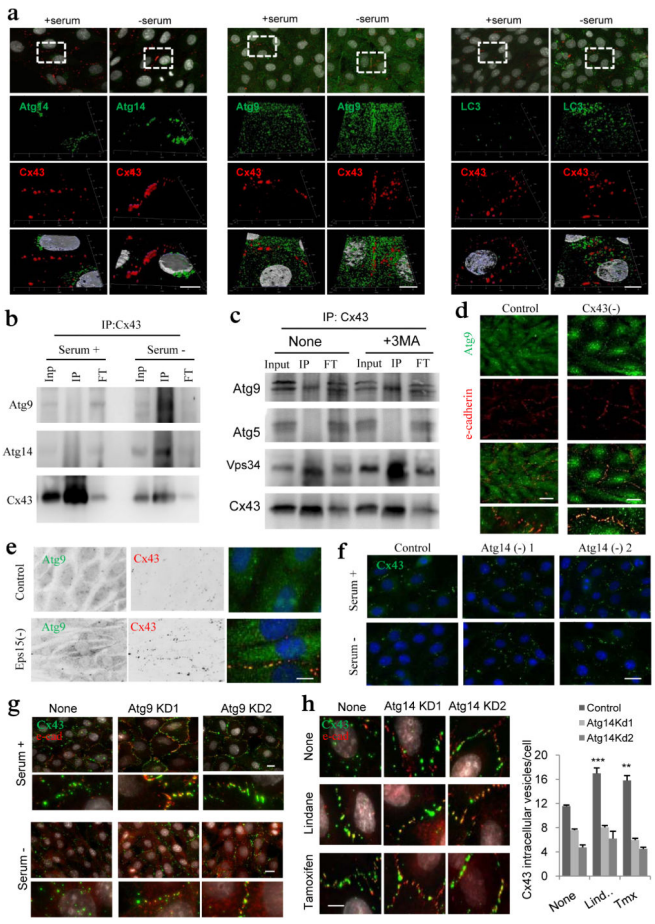

Figure 7. Cx43 modulates formation of pre-autophagosomal structures through direct interaction with autophagy-related proteins

(**a**) Co-immunostaining for Cx43 and the indicated Atgs in NRK cells maintained in the presence or absence of serum (top). Single and merged channels of the 3D reconstruction of the boxed regions are shown (bottom). Nuclei are highlighted with DAPI. (**b, c**) Immunoblot for the indicated proteins of immunoprecipitates (IP) of Cx43 in NRK cells maintained in the presence or absence of serum (**b**) or treated or not with 3-methyladenine (**c**) Atg5 is shown as negative control for IP. (**d**) Co-staining for Atg9 and e-cadherin in NRK cells control and knocked down for Cx43. Single and merged channels at higher magnification areas are shown. (**e**) Immunofluorescence for endogenous Atg9 and Cx43 in NRK cells control or knocked down for Eps15. (**f, g**) Immunofluorescence for endogenous Cx43 (green) in NRK cells control or knocked down for Atg14 (**f**) or Atg9 (**g**) maintained in the presence or absence of serum. (**h**) Immunofluorescence of endogenous Cx43 in NRK cells control or knocked down for Atg14 treated (or not) with Tx or Lnd (left). e-cadherin staining (red) is shown to highlight plasma membrane in **g** and **h**. Full fields are shown in Supplementary Fig. 6h. Quantification of intracytoplasmic Cx43-positives vesicles (right) (n= 3 wells, 3 independent experiments, >30 cells per experiment). Values are mean+s.e.m and significant for (*) $p<0.01$ using ANOVA+Bonferroni test. Bars: 5 μm. Uncropped images of blots are shown in Supplementary Fig. 9.

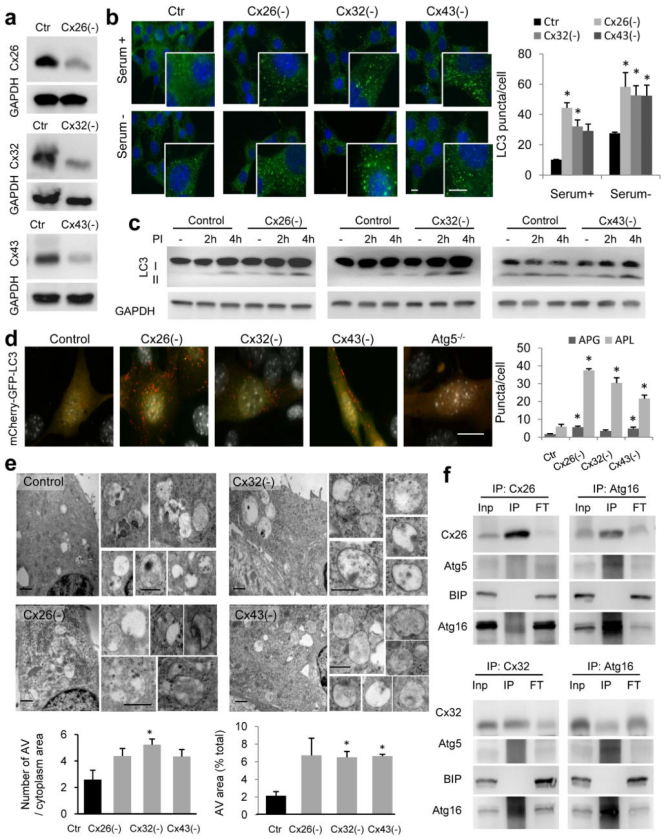

Figure 8. Depletion of connexins induces autophagosome formation

(**a**) Immunoblot for the indicated proteins in mouse embryonic fibroblasts (MEFs) control or knocked down (−) for the three different connexins. (**b**) Immunofluorescence of LC3 in MEFs control (Ctr) or knocked down (−) for three different Cx maintained in the presence or absence of serum. Left: representative fields and higher magnification insets. Nuclei are highlighted with DAPI. Right: Quantification of the average number of LC3-positive puncta per cell (n= 3 wells, 3 independent experiments, >50 cells per experiment). **(c)** Immunoblot for LC3 in the same cells maintained in the presence of serum untreated (−) or treated with inhibitors of lysosomal proteases (PI) for the indicated times. GAPDH is shown as loading control. (**d**) Representative images of MEFs control or knocked-down (−) for the indicated proteins transfected with the mCherry-GFP-LC3 tandem reporter. Right: quantification of the average number per cell of puncta positive for GFP and mCherry (autophagosomes; APG) and those positive only for mCherry (autophagolysosomes; APL) (n= 3 wells, 3 independent experiments, >50 cells per experiment). (**e**) Electron micrographs of MEFs control or knock-down for the indicated Cx. Insets show autophagic vesicles. Bottom: Quantification of the average number of AV (left) and percentage of cytosolic area (right) occupied by AVs (n= 4 wells, 4 independent experiments, >10 micrographs per well). (**f**) Immunoblot for indicated proteins in immunoprecipitates (IP) for Cx26 or Cx32 (left) or Atg16 (right) from liver homogenates. Inp: input, FT: flow through. BIP is shown as negative control for IP. All values are mean+s.e.m and significant for (*) $p<0.01$ (ANOVA

+Bonferroni test was used in b). Bars: 5 μm in fluorescence images; 1 μm and 0.1 μm in top panels and inserts of e. Uncropped images of blots are shown in Supplementary Fig. 9.